Heat Effects in Gas Sulfiding of Hydroprocessing Catalysts

An *a priori* model is developed to assess the heat effects during gas-phase (H_2S/H_2) sulfiding of a $CoO—MoO_3/\gamma—Al_2O_3$ hydroprocessing catalyst in a small fixed-bed reactor. The model satisfactorily predicts the observed maximum temperature rise and the speed of the traveling exotherm. It is found that the amount of heat released can be of sufficient magnitude to cause significant hot spotting and local starvation of H_2S, both of which need to be avoided for desired catalyst performance. With this model, parametric studies were made to optimize the sulfiding operation. It is expected that the model can be used to guide catalyst synthesis research and to scale up laboratory/pilot-plant sulfiding procedures.

S. C. Reyes, T. C. Ho
Corporate Research Laboratories
Exxon Research and Engineering Company
Annandale, NJ 08801

Introduction

The need to produce processible and clean liquid fuels from low-quality hydrocarbon feedstocks has stimulated numerous investigations into the fundamentals of hydroprocessing catalysis. Essentially two types of catalysts, $CoO—MoO_3/\gamma—Al_2O_3$ and $NiO—MoO_3/\gamma—Al_2O_3$, are in use in present-day refineries. Prior to use, the catalysts must be sulfided with a sulfur-bearing stream, so that at least part of the oxide ions in the catalyst are replaced by the more active and stable sulfur ions. The reaction is highly exothermic and therefore needs to be carefully controlled. It is well known that the performance of commercial catalysts is strongly dependent on how the sulfiding is carried out, as witnessed by the voluminous patent literature on this subject.

Commercial sulfiding technologies generally fall into four broad categories (Hallie, 1982; Riddick and Peralta, 1980; Berrebi, 1985):

1. Those that use an H_2S/H_2 gas mixture in contact with the catalyst
2. Those that use the native organic sulfur compounds in the feedstock
3. Those that spike the feedstock with a sulfur-donating species (e.g., mercaptans, thioethers, carbon disulfide, etc.)
4. Those that impregnate the catalyst *ex situ* with a sulfur-containing compound (e.g. ammonium sulfide)

In laboratory or pilot-plant studies, it is quite common to use an H_2S/H_2 gas mixture as the sulfiding agent. Liquid sulfiding is considerably slower than gas sulfiding.

Gas sulfiding in general is accompanied by significant hot spotting due to low gas heat capacity and high reaction exothermicity. The temperature profiles generated during catalyst sulfiding are fairly complex. Consider a downflow fixed-bed reactor. At the start of the experiment, the top layers of the bed contact a high concentration of incoming H_2S and get sulfided. This consumes a significant amount of H_2S and causes a high-temperature rise. Meanwhile, the bottom layers of the bed may be starved of H_2S. Once the front end of the catalyst bed becomes sulfided, the heat liberation falls and the hot spot will move down the bed. Thus, here one deals with a system exhibiting a traveling hot spot. In catalyst activity-structure studies, it is essential to know the exact conditions to which the catalyst has been subjected during sulfiding. And it is highly desirable to be able to control the sulfiding conditions because hot spotting and/or H_2S starvation can damage the catalyst.

Surprisingly enough, to date no quantitative studies on sulfiding of hydroprocessing catalysts seem to have appeared in the open literature. Accordingly, the purpose of this work was to develop a mathematical model for gas (H_2S/H_2) sulfiding of a commercial hydroprocessing catalyst in a small fixed-bed reactor. The intrinsic sulfiding kinetics were determined by using a thermogravimetric analyzer. Fixed-bed sulfiding experiments were done to measure the traveling temperature profiles against which the model was tested.

This paper is organized as follows. We begin with a brief description of the experimental part of the work. We then develop perhaps the simplest mathematical model capturing the essential features of catalyst sulfiding. With this model, the time evolution of metal oxide concentration as well as other nonob-

*Correspondence concerning this paper should be addressed to T. C. Ho.

servable quantities of interest are predicted. These predictions suggest that the extent of local hot spotting and H_2S starvation can be quite significant. Finally, we conclude our analysis with a parametric study aimed at optimizing the sulfiding operation.

Experimental Procedure

Catalyst

The catalyst used in this study is a typical CoO—MoO_3/γ—Al_2O_3 catalyst with the following nominal composition and physical properties: CoO, 4%; MoO_3, 16%; surface area, 165 m^2/g; pore volume, 0.65 cm^3/g.

Thermogravimetric analysis

A Mettler TGA apparatus (model TA 2000 C) used in this study for determining the sulfiding kinetics is diagramed in Figure 1. The main components of this apparatus include a vertical tube furnace *A*, balance *B*, and rotary pump *C*. The catalyst sample, *D*, was suspended inside the tube furnace. The H_2S/H_2 gas mixture (supplied by Matheson) with the desired composition was introduced slowly from the top of the reaction tube *E*. Its flow rate was controlled by a Tylan mass flow controller. The reacted gas was allowed to exit the system through a side arm *F* located at the lower portion of the furnace. The electronic part (including the balance) of the apparatus was blanketed with flowing He, which also exits the system through the side arm. The flow rates of the gaseous mixtures in the system are such that there is minimum mixing between H_2S/H_2 and He. The electronic output signals corresponding to the weight changes were recorded on a strip-chart recorder as a function of reaction time. The temperature in the hot zone was measured by a sheathed type K thermocouple situated right below the sample.

In a typical experiment, a catalyst sample of about 65 mg was placed in a ceramic cup. The system was then evacuated to approximately 10^{-2} torr (1.33×10^{-3} kPa). Following this, a stream of He was introduced into the system and the furnace was heated to the desired temperature at atmospheric pressure. Once the sample weight change stabilized, the He flow was redirected and a mixture of 10% H_2S/H_2 was slowly introduced at ca. 25 cm^3/min at about 30°C, which formed the starting point of the run. The run was continued until the sample showed no further discernible weight changes. The flow of H_2S/H_2 was then terminated and He was introduced to flush out any remaining H_2S/H_2. The furnace was then allowed to cool to room temperature.

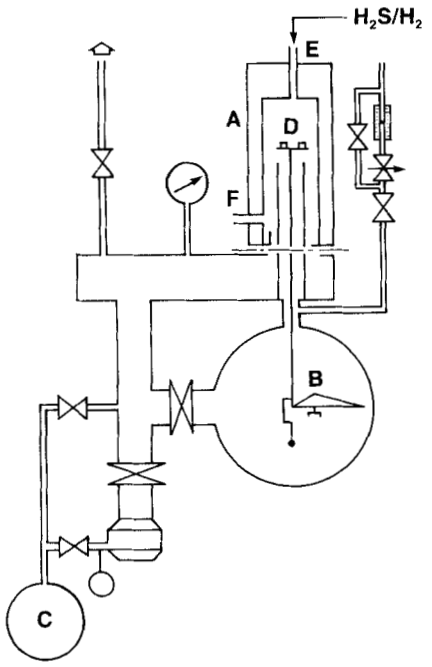

Figure 1. Thermogravimetric analyzer.

Catalyst sulfiding in fixed-bed reactor

Nonisothermal and nonadiabatic sulfiding experiments were carried out in a fixed-bed reactor made of 1 in. (25.4 mm) OD 316 stainless steel tube. The reactor was equipped with a Tylan mass flow controller and thermowell with a movable thermocouple. Heating was supplied and regulated by an electrical furnace to maintain a nearly constant wall temperature. The effluent gas was passed through a caustic scrubber to remove H_2S. The total pressure of the system was held at 1.0 atm.

An experimental run was typically carried out as follows. Approximately 70 cm^3 of the catalyst sample was loaded in the reactor. The reactor was then purged with nitrogen at 100°C for 1 h. The reactor wall temperature was then raised to 400°C and kept at this temperature for at least 30 min. At time zero, the nitrogen flow was stopped and a gas mixture containing 10% H_2S/H_2 was admitted to the reactor at a rate of 800 cm^3/min, at room temperature. The reactor temperature profiles were then measured by moving the thermocouple in the thermowell at different sulfiding times. When the sulfiding reaction was completed—as indicated by the flattening of the temperature profile—the flow of H_2S/H_2 and heating of the tube were terminated and the reactor was purged with nitrogen until room temperature was reached.

Sulfiding Kinetics

The mechanism of catalyst sulfiding is still poorly understood, although the subject has been investigated by many (Massoth, 1975; Arnoldy et al., 1985). There appears to be no general agreement on the details of the reaction pathways. It has been proposed that the conversion of MoO_3 to MoS_2 involves the formation of MoO_2 (Arnoldy et al., 1985) and/or MoS_3 as intermediates (Hallie, 1982). The reduction of MoO_3 to MoO_2 is believed to be much faster than the sulfiding reactions. The sulfiding of CoO most likely involves several reactions, resulting in formation of such phases as Co_9S_8, $CoAlO_4$, and a so-called "Co—Mo—S" species (Topsøe and Clausen, 1984). Besides the oxide ions that are replaced by the sulfide ions, additional oxide ions may be lost by reduction with hydrogen. This leads to the formation of anion vacancies whose concentration is believed to be very low (Massoth, 1975).

Due to the lack of fundamental information on sulfiding reaction pathways, it was decided to lump MoO_3 and CoO together as a single entity whose rate of weight change was taken as the rate of sulfiding. The overall sulfiding reaction may be written as

$$(MoO_3 + CoO) + 2\tfrac{8}{9}H_2S + 1\tfrac{1}{9}H_2 \rightarrow (MoS_2 + \tfrac{1}{9}Co_9S_8) + 4H_2O \quad (1)$$

This reaction stoichiometry, while constituting an oversimplification of reality, is believed to be a good first approximation as far as modeling the reactor temperature profiles is concerned. Equation 1 indicates that the sulfiding reaction essentially involves no volume change, and that the reaction results in a net weight gain because S is heavier than O.

The effect of intraparticle transfer resistances was studied by running the TGA experiments at a high temperature of 430°C using two different particle sizes, 20/40 and 100/200 mesh sizes. The two sets of weight gain data practically coincided. In the kinetic analysis to follow we neglect intraparticle transfer resistances.

The weight gain data obtained at three different temperatures, 380, 400, and 430°C, are presented in Figure 2 as plots of $\ln(1 - W)$ vs. time where W is the fractional weight gain. From these plots, it can be seen that the sulfiding reaction can be reasonably considered to be first order with respect to the metal oxide concentration. The rate constants at different temperatures were then determined from the slopes of these plots. Figure 3 shows the corresponding Arrhenius plot. The activation energy was determined as 235.6 kJ/mol (56.3 kcal/mol), indicating that sulfiding of this catalyst is a highly activated process.

The dependence on H_2S concentration was assumed to be first order because gas sulfiding in practice is generally conducted with an H_2S/H_2 mixture containing a limited amount of H_2S, say up to 10 vol. %. Within this concentration range, the reaction can reasonably be assumed to be first order in H_2S concentration. Tamhankar et al. (1981) have found sulfiding of iron oxides to be first order in H_2S concentration. Richardson (1971) and Weng et al. (1975) each have observed a first-order dependence in related studies.

The following expression for the rate constant, with units of $m^3/kg \cdot mol/s$, summarizes the results on sulfiding kinetics:

$$k = k_o \exp(-E/RT) = 3.4 \times 10^{18} \exp\left(-\frac{235.6 \text{ kJ/mol}}{R_g T}\right) \quad (2)$$

Modeling of Sulfiding Reactor

Since the sulfiding experiments were carried out in a small reactor, a one-dimensional axial dispersion model is used. By using Mears' (1971) criterion on interphase transfer resistances, we found that sizable concentration and temperature gradients could develop between the gas and the solid. We neglect heat conduction along the wall and heat generation due to metal oxide reduction with H_2 (which has a small heat of reaction). With the usual assumption of constant physical properties, we thus have:

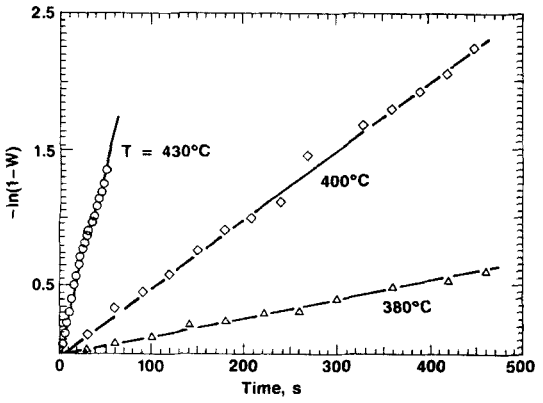

Figure 2. First-order kinetic plot for catalyst sulfiding.

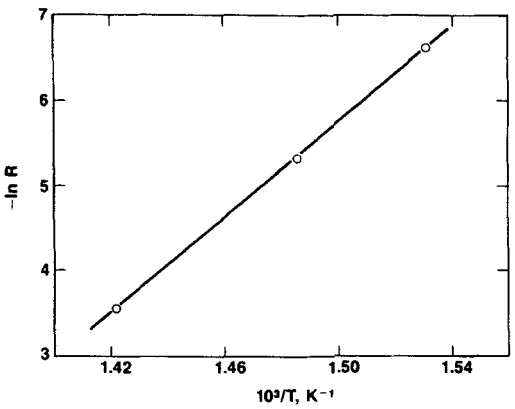

Figure 3. Arrhenius plot of rate constants for catalyst sulfiding.

H_2S Balance for Reactor

$$\epsilon \frac{\partial C}{\partial t} + U \frac{\partial C}{\partial z'} = D \frac{\partial^2 C}{\partial z'^2} - k_g a_v (C - C_s) \quad (3)$$

Energy Balance for Reactor

$$\epsilon \rho_g C_{pg} \frac{\partial T}{\partial t} + U \rho_g C_{pg} \frac{\partial T}{\partial z'} = \lambda \frac{\partial^2 T}{\partial z'^2} + h_f a_v (T_s - T) - \frac{2h}{r_T}(T - T_c) \quad (4)$$

H_2S Balance for Catalyst Particle

$$\epsilon_s (1 - \epsilon) \frac{\partial C_s}{\partial t} = k_g a_v (C - C_s) - \rho_b R \quad (5)$$

Energy Balance for Catalyst Particle

$$(1 - \epsilon) \rho_s C_{ps} \frac{\partial T_s}{\partial t} = -h_f a_v (T_s - T) + (-\Delta H) \rho_b R \quad (6)$$

Mass Balance for Metal Oxides

$$\frac{\partial n}{\partial t} = -R = -k_o n C_s \exp(-E/R_g T_s) \quad (7)$$

We now wish to nondimensionalize the above equations, bearing in mind that we are mainly interested in the "steady" movement of the heat front in the bed. We therefore choose a slow time scale on which the reaction heat is transferred from the catalyst to the gas. This leads to the following scaled dimensionless time

$$\tau = \frac{t h_f a_v}{(1 - \epsilon) \rho_s C_{ps}} \quad (8)$$

Having selected the relevant time scale, we nondimensionalize Eqs. 3–7 in the usual manner by introducing the following variables:

$$x = 1 - C/C_o \quad y = 1 - C_s/C_o \quad S = n/N_s \quad z = z'/L$$

$$u = \frac{T - T_c}{T_c} \quad v = \frac{T_s - T_c}{T_c} \quad u_o = T_o/T_c \quad \alpha = \frac{k_g a_v L}{U}$$

$$\beta = \frac{h_f a_v L}{U \rho_g C_{pg}} \quad \gamma_o = \frac{2hL}{U \rho_g C_{pg} r_T} \quad \delta = \frac{\rho_b N_s k_o}{k_g a_v}$$

$$\epsilon_o = \frac{(-\Delta H)\rho_b C_o k_o N_s}{T_c h_f a_v}$$

$$\xi = \frac{k_o C_o (1 - \epsilon)\rho_s C_{ps}}{h_f a_v} \quad \gamma = \frac{E}{RT_c} \quad Pe_m = \frac{UL}{D}$$

$$Pe_h = \frac{U \rho_g C_{pg} L}{\lambda}$$

$$\Theta_o = \frac{\epsilon L}{U} \frac{h_f a_v}{(1 - \epsilon)\rho_s C_{ps}}$$

$$\Theta_1 = \frac{\epsilon_s (1 - \epsilon)}{k_g a_v} \frac{h_f a_v}{(1 - \epsilon)\rho_s C_{ps}}$$

Under conditions of practical interest, Θ_o and Θ_1 are both $\ll 1$; that is, the bulk gas temperature and the H_2S concentrations in gas and catalyst are at a quasi-steady state on the time scale over which catalyst temperature changes. We thus obtain the following quasi steady-state model in dimensionless form, which represents the zeroth approximation to the full problem defined by Eqs. 3–7.

$$O = -\frac{\partial x}{\partial z} + \frac{1}{Pe_m}\frac{\partial^2 x}{\partial z^2} + \alpha(y - x) \tag{9}$$

$$O = -\frac{\partial u}{\partial z} + \frac{1}{Pe_h}\frac{\partial^2 u}{\partial z^2} + \beta(v - u) - \gamma_o u \tag{10}$$

$$O = x - y + \delta S(1 - y)\exp[-\gamma/(v + 1)] \tag{11}$$

$$\frac{\partial v}{\partial \tau} = u - v + \epsilon_o S(1 - y)\exp[-\gamma/(v + 1)] \tag{12}$$

$$\frac{\partial S}{\partial \tau} = -\xi S(1 - y)\exp[-\gamma/(v + 1)] \tag{13}$$

The pertinent initial and boundary conditions are:

$$\frac{1}{Pe_m}\frac{dx}{dz} = x, \quad z = 0 \tag{14}$$

$$\frac{dx}{dz} = 0, \quad z = 1 \tag{15}$$

$$\frac{1}{Pe_h}\frac{du}{dz} = u - u_o + 1, \quad z = 0 \tag{16}$$

$$\frac{du}{dz} = 0, \quad z = 1 \tag{17}$$

$$v(z, \tau) = 0, \quad \tau = 0 \tag{18}$$

$$S(z, \tau) = 1, \quad \tau = 0 \tag{19}$$

The model predictions presented in the sections to follow were obtained by numerically solving the above equations via orthogonal collocation on finite elements (Carey and Finlayson, 1975). The resulting system of differential and algebraic equations were simultaneously solved by integrating forward in time with EPISODE (Hindmarsh and Byrne, 1975) and the Newton-Raphson method, the convergence of which was accelerated by a first-order continuation scheme.

Comparison with Experimental Data

Table 1 summarizes the sulfiding conditions used in this study, along with the corresponding physical constants and parameter values used in the numerical computations. The parameter values were estimated from existing correlations (Froment and Bischoff, 1979; Reid et al., 1977). Figure 4 shows the observed and predicted (solid lines) temperature profiles for an inlet temperature T_o of 392°C and a wall temperature T_c of 400°C. As can be seen, the model satisfactorily predicts the speed of the traveling heat front as well as the magnitude of the temperature rise. However, some overpredictions are observed near the reactor end points. Possible reasons for this discrepancy include:

1. Heat losses at the reactor end points due to too short a reactor length
2. Heat conduction along the reactor wall
3. Reduction of metal oxides with hydrogen

It was considered unnecessary to refine the model to account for these effects because our main concerns here are the magnitude of the temperature rise and the speed of the traveling heat front. We therefore consider the model reasonably predictive. In this regard, it may be emphasized that the parameter values in the model were all obtained from existing correlations. And with the same parameter values, we were able to predict the sulfiding

Table 1. Experimental Conditions, Physical Constants, and Parameter Values Used in Reactor Modeling

Reactor length	$L = 0.1524$ m
Reactor radius	$r_T = 0.0102$ m
Bed void fraction	$\epsilon = 0.30$
Superficial velocity	$U = 0.136$ m/s
Overall heat transfer coefficient	$h = 0.05$ kJ/m^2·s·°C
Heat of reaction	$-\Delta H = 154.8$ kJ/mol
Molar ratio in feed	$X_{H_2S}/X_{H_2} = 1/9$
Gas heat capacity	$C_{pg} = 4.39$ kJ/kg·°C
Solid heat capacity	$C_{ps} = 0.96$ kJ/kg·°C
Peclet number for mass	$Pe_m = 109$
Peclet number for heat	$Pe_h = 27$
Solid concentration	$N_s = 6.94$E-4 kmol/kg cat
Solid density	$\rho_p = 1{,}100$ kg/m^3
Particle size	$d_p = 20/40$ mesh
Preexponential factor	$k_o = 3.4$E18 kmol/m^3·s
Activation energy	$E = 235.6$ kJ/mol
Mass transfer coefficient	$k_g a_v = 5.0$ 1/s
Heat transfer coefficient	$h_f a_v = 20.9$ kJ/m^3·s·°C

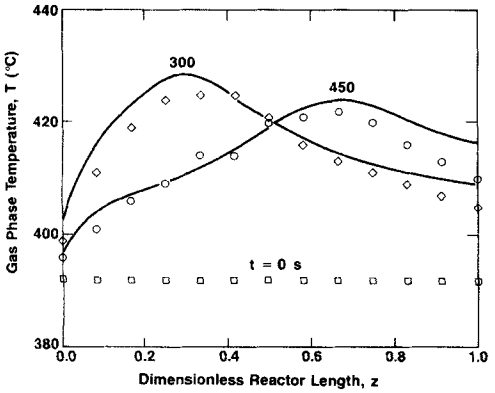

Figure 4. Experimental and predicted gas temperature profiles in reactor.

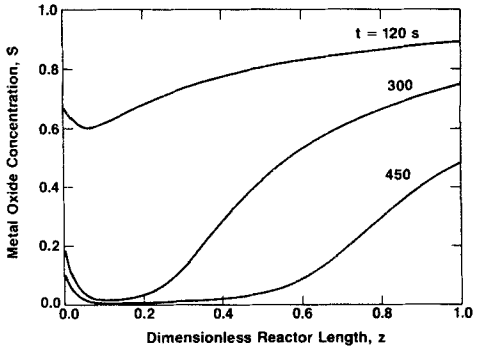

Figure 6. Predicted profiles of metal oxide concentration.

behavior of a self-made Co—Mo oxide catalyst that gives rise to a much more severe hot spotting and local starvation of H_2S (Reyes and Ho, 1986).

Figure 5 shows the predicted gas temperature profiles during the early stages of the operation. As can be seen, the gas temperature can be some 40°C higher than the inlet temperature. This hot spotting could cause significant damage to the catalyst, as will be discussed in some detail later.

We next use the model to predict the evolution of some nonobservable quantities of interest: the concentration of metal oxides, the concentrations of H_2S in the gas and catalyst, and the particle temperature.

Figure 6 illustrates the traveling profiles of the metal oxide concentration. It can be observed that in the reactor there is a region within which the concentration of metal oxide first decreases and then increases. Note also that the top few layers of the catalyst bed remain incompletely sulfided even after 450 s. This behavior is due to an interplay between heat piling and reactant consumption: The heat generated by sulfiding of the first catalyst layer will heat up the gas and the catalyst layer next to it. This will in turn enhance the sulfiding rate (which has a high activation energy), causing more heat generation and a further decrease in the oxide concentration. As this proceeds, sooner or later the rate will start to slow down because of the depleting H_2S concentration. As the reaction rate gets slower, the oxide concentration will eventually go up. This is consistent with the prediction that the magnitude of the gas temperature wave grows initially, Figure 5, reaches an absolute maximum at a particular point in the bed at a particular time, and then decreases, Figure 4. As will be discussed later, an important consideration in designing sulfiding procedures is this absolute maximum temperature rise. Another point to note is that the heat front, because of the convective effect of gas flow, moves faster than the solid concentration wave.

Shown in Figure 7 are the H_2S breakthrough curves. The H_2S concentration reaches an absolute minimum at the reactor outlet at a particular time. During the initial stages of the operation, the H_2S levels are rather low near the reactor outlet. Sulfiding of catalysts in an H_2S-starved environment can lead to an undesirable change in catalyst structure: An environment initially rich in H_2 may cause a deep reduction of the metal oxides, resulting in undesired agglomeration of the active metals. These massive agglomerates, upon sulfiding with H_2S at later times, may form large metal sulfide crystallites of a low activity. When this occurs, the active metals are underutilized. Riddick and Peralta (1980) used a similar mechanism to rationalize their sulfiding data.

As mentioned before, interfacial transport resistances should be important in the present system. We verified this by using a pseudohomogeneous model, which resulted in significant overpredictions of the gas temperature and, consequently, the speed of the temperature wave. Figures 8 and 9 show the temperature and H_2S concentration differences between the gas and the catalyst particle, respectively. The behavior seen here can be rationalized by the coupled heat-piling and reactant-consumption effects discussed earlier. The extent of local overheating of the catalyst particles can be seen by the following numerical result. At t = 300 s the catalyst located about one-third way down the

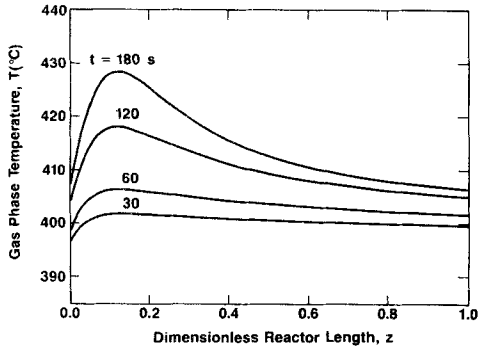

Figure 5. Predicted gas temperature profiles during early stages of catalyst sulfiding.

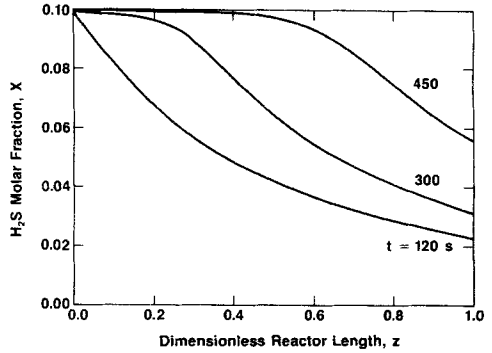

Figure 7. Breakthrough cruves for H_2S.

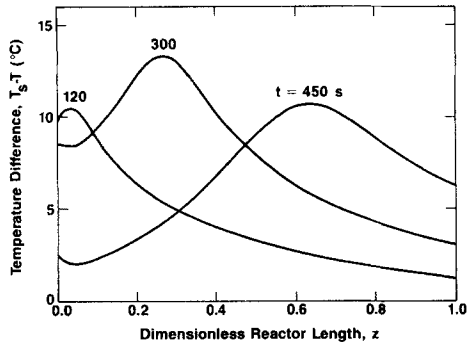

Figure 8. Calculated temperature difference between gas and catalyst.

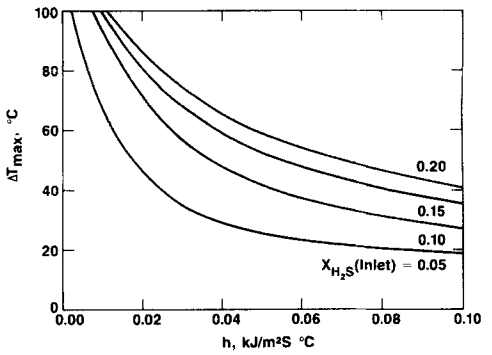

Figure 10. Effect of overall heat transfer coefficient on absolute maximum temperature rise ΔT_{max}.

bed ($z \sim 0.3$) will be some 13°C hotter than the gas. This temperature difference is quite significant in view of the facts that the sulfiding reaction has a high activation energy and that the gas at that point is hotter than the inlet gas by about 40°C.

Parametric Studies

We now perform some numerical scoping studies using the model. Since the structure of the catalyst is mainly dependent on temperature and H_2S concentration, one normally needs to design the sulfiding procedure subject to an upper bound on the absolute maximum temperature rise ($\Delta T_{max} \leq \Delta \bar{T}_{max}$) and a lower bound on the absolute minimum H_2S concentration ($X_{min} \geq \bar{X}_{min}$). Figures 10 and 11 show the predicted ΔT_{max} and X_{min}, respectively, as a function of the overall heat transfer coefficient h for different H_2S inlet concentrations (mole fraction). Suppose that we arbitrarily select $\Delta \bar{T}_{max} = 60$°C and $\bar{X}_{min} = 0.01$, we can then define the allowable operating region by combining Figures 10 and 11. This is shown in Figure 12 by the area enclosed by curves A and B. Curve A is the trajectory for $\Delta T_{max} = 60$°C, which is a replot of all the $\Delta T_{max} = 60$°C points in Figure 10. The dashed lines correspond to the various H_2S inlet concentrations. Since the absolute maximum temperature rise is a measure of the sulfiding rate, for a given reaction time the conversion of metal oxides, or productivity, increases in the perpendicular direction to curve A. Although a number of combinations of H_2S inlet concentrations and heat transfer coefficients can be operated along curve A for maximum productivity, the optimum operating point should be the intersection between curves A and B. At this point, both constraints ($\Delta \bar{T}_{max} = 60$°C and $\bar{X}_{min} = 0.01$) are satisfied, and the overall conversion of H_2S is maximized.

It is important to note that because the constraints discussed above are critical only at early times during sulfiding, the productivity can be further increased by properly programming the time progression of the gas inlet temperature and/or the wall temperature. Although not further detailed here, we have verified this by using the model to determine the productivity for temperature-programmed operations. As expected, changes in T_c play a more important role than changes in T_o because of the low heat capacity of the gas.

Conclusions

The approach described in the present study represents a first step toward a quantitative understanding of sulfiding of hydroprocessing catalysts. It is found that the axial temperature gradient in a small sulfiding reactor can be very large. It is thus important to monitor the reactor temperature along the bed. The catalyst particles can be much hotter than the bulk gas. These heat effects can give rise to severe local hot spotting and H_2S starvation. Failure to quantify the heat effects in catalyst sulfiding can lead to erroneous conclusions regarding the structure and performance of the catalyst.

It is expected that the model can be used for guiding hydroprocessing catalyst research as well as for scaling up laboratory/pilot-plant sulfiding procedures.

Notation

a_v = interfacial area, m^2/m^3
C = gas concentration, $kmol/m^3$

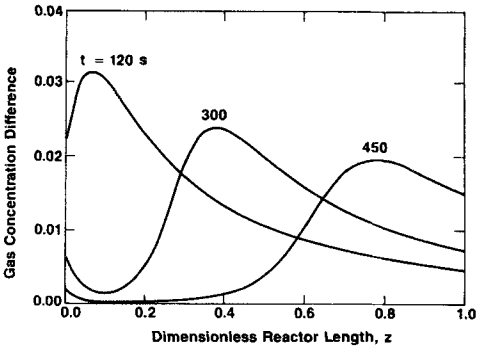

Figure 9. Calculated H_2S concentration difference between gas and catalyst.

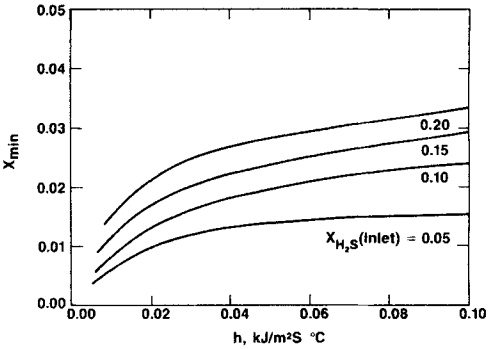

Figure 11. Effect of overall heat transfer coefficient on absolute minimum H_2S molar fraction X_{min}.

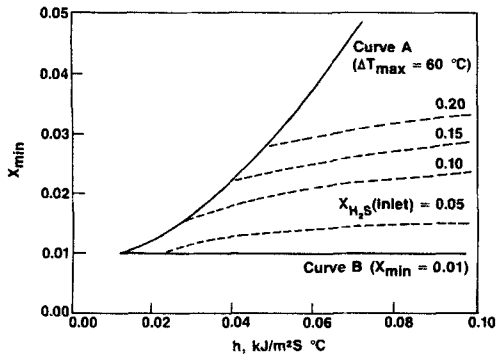

Figure 12. Permissible sulfiding region and optimum sulfiding conditions.

C_p = heat capacity, kJ/kg · °C
D = diffusion coefficient, m^2/s
d_p = particle diameter, m
E = activation energy, kJ/mol
h = overall heat transfer coefficient, kJ/s · m^2 · C
h_f = interfacial heat transfer coefficient, kJ/s · m^2 · °C
k = kinetic rate constant, m^3/kmol · s
k_o = preexponential factor, m^3/kmol · s
k_g = interfacial mass transfer coefficient, m/s
L = reactor length, m
n = solid concentration, kmol/kg · cat
N_s = initial solid concentration, kmol/kg cat
P_e = Peclet number
R = reaction rate, kmol/kg cat · s
R_g = gas constant, kJ/kmol · K
r_T = reactor radius, m
S = dimensionless solid concentration
t = time, s
T = absolute temperature, K
T_c = wall temperature
T_o = inlet temperature
u = dimensionless gas temperature
U = superficial velocity, m/s
u_o = dimensionless inlet temperature
v = dimensionless solid temperature
w = fractional weight gain
X = H_2S mole fraction
x = gas conversion in bulk phase
y = gas conversion in solid phase
z = dimensionless axial reactor distance
z' = axial reactor distance, m

Greek letters

α = dimensionless variable
β = dimensionless variable
γ = dimensionless activation energy
γ_o = dimensionless variable
δ = dimensionless variable
Δ = difference
ΔH = heat of reaction, kJ/mol
ϵ = bed void fraction
ϵ_o = dimensionless variable
Θ_1 = dimensionless variable
Θ_2 = dimensionless variable
λ = thermal conductivity, kJ/s · m · °C
ξ = dimensionless variable
ρ_g = gas density, kg/m^3
ρ_p = particle density, kg cat/m^3 cat

Subscripts

b = bulk phase
g = gas phase
h = heat
m = mass
max = maximum
min = minimum
s = solid

Literature Cited

Arnoldy, P., J. A. M. van den Heijkant, G. D. de Bok, and J. A. Moulijn, "Temperature-Programmed Sulfiding of MoO_3/Al_2O_3 Catalysts," *J. Catal.*, **92,** 35 (1985).

Berrebi, G., "Presulfiding of Hydrocarbon Treatment Catalysts," Eur. Pat. Appl. 153233, assigned to Eurecat (1985).

Carey, G. F., and B. A. Finlayson, "Orthogonal Collocation on Finite Elements," *Chem. Eng. Sci.*, **30,** 587 (1975).

Froment, G. F., and K. B. Bischoff, *Chemical Reactor Analysis and Design,* Wiley, New York (1979).

Hallie, H., "Experience Reveals Best Presulfiding Techniques for HDS and HDN Catalysts," *Oil Gas J.*, 69 (Dec.,1982).

Hindmarsh, A. C., and G. D. Byrne, "EPISODE: An Experimental Package for the Integration of Systems of ODE's," Lawrence Livermore Lab. Rep. UCID-30112 (1975).

Massoth, F. E., "Studies of Molybdena-Alumina Catalysts. IV: Rates and Stoichiometry of Sulfidation," *J. Catal.*, **36,** 164 (1975).

Mears, D. E., "Tests for Transport Limitations in Experimental Catalytic Reactors," *Ind. Eng. Chem. Process Des. Dev.*, **10,** 541 (1971).

Reid, R. C., J. M. Prausnitz, and T. K. Sherwood, *The Properties of Gases and Liquids,* McGraw-Hill, New York (1977).

Reyes, S. C., and T. C. Ho, "Mathematical Modeling and Experimental Study of Sulfiding of Hydroprocessing Catalysts," *AIChE Ann. Meet.*, Miami Beach (1986).

Richardson, J. T., "Sulfiding of Nickel Catalyst Beds," *J. Catal.*, **21,** 130 (1971).

Riddick, F. C., Jr., and B. Peralta, "Hydrodesulfurization of Oil Feedstock with Presulfided Catalysts," U.S. Pat. 4213850, assigned to Union Oil Co. of California (1980).

Tamhankar, S. S., M. Hasatani, and C. Y. Wen, "Kinetic Studies on the Reactions Involved in the Hot Gas Desulfurization Using a Regenerable Iron Oxide Sorbent. I," *Chem. Eng. Sci.*, **36,** 1181 (1981).

Topsøe, H., and B. S. Clausen, "Importance of Co—Mo—S Type Structures in Hydrodesulfurization," *Catal. Rev.-Sci. Eng.*, **26,** 395 (1984).

Weng, H. S., G. Eigenberger, and J. B. Butt, "Catalyst Poisoning and Fixed-Bed Reactor Dynamics," *Chem. Eng. Sci.*, **30,** 1341 (1975).

Manuscript received Jul. 29, 1987, and revision received Oct. 23, 1987.